A natural O-ring optimizes the dispersal of fungal spores

Joerg A. Fritz, Agnese Seminara, Marcus Roper, Anne Pringle, Michael P. Brenner

A natural O-ring optimizes the dispersal of fungal spores

Joerg Fritz[*†] Agnese Seminara[*] Marcus Roper[‡]
Anne Pringle[§] Michael P. Brenner[*]

July 17, 2013

Abstract

The forcibly ejected spores of ascomycete fungi must penetrate several millimeters of nearly still air surrounding sporocarps to reach dispersive airflows, and escape is facilitated when a spore is launched with large velocity. To launch, the spores of thousands of species are ejected through an apical ring, a small elastic pore. The startling diversity of apical ring and spore shapes and dimensions make them favored characters for both species descriptions and the subsequent inference of relationships among species. However, the physical constraints shaping this diversity and the adaptive benefits of specific morphologies are not understood. Here, we develop an elastohydrodynamic theory of the spore's ejection through the apical ring, and demonstrate that to avoid enormous energy losses during spore ejection, the four principal morphological dimensions of spore and apical ring must cluster within a nonlinear one-dimensional subspace. We test this prediction using morphological data for 45 fungal species from two different classes and seventeen families. Our sampling encompasses multiple loss and gain events and potentially independent origins of this spore ejection mechanism. Although the individual dimensions of the spore and apical ring are only weakly correlated with each other, they collapse into the predicted subspace with high accuracy. The launch velocity appears to be within 2% of the optimum for over 90% of all forcibly ejected species. Although the morphological diversity of apical rings and spores appears startlingly diverse, a simple principle can be used to organize it.

[*]School of Engineering and Applied Sciences and Kavli Institute for Bionano Science and Technology, Harvard University, Cambridge, MA 02138, USA

[†]To whom correspondence should be addressed. E-mail:jfritz@seas.harvard.edu

[‡]Department of Mathematics, University of California, Los Angeles, 90095, CA, USA

[§]Department of Organismic and Evolutionary Biology, Harvard University, Cambridge, MA 02138, USA

Spore dispersal is the primary determining factor for the range and distribution of fungi in nature. The importance of understanding this process in detail has been highlighted in recent years by an unprecedented number of fungal diseases, which have caused some of the most severe die-offs and extinctions ever witnessed in wild species [1], and are increasingly considered a worldwide threat to food security [2]. An effective control of these emerging diseases is only possible if we can understand and control how they propagate.

The defining feature of the largest fungal phylum, Ascomycota, is the ascus, a fluid filled sac from which spores are ejected. Ejection is powered by a buildup of osmotic pressure [3], which forces spores through a ring or hole at the tip of the ascus, after a critical pressure is reached [4]. Ascus and spore morphologies are highly variable, and have been an essential element of species descriptions for more than 200 years [5, 6]. Since spores are the primary agents of dispersal, these morphologies also play a critical role in the ascomycete life cycle: most fungi grow on highly heterogeneous landscapes, and to persist a fungus must move between disjoint patches of habitat [7], thus effective dispersal is critical to the fitness of an individual.

To reach dispersive air currents, spores must be launched with enough speed to cross the stagnant air layer around the fungus, the fluid mechanical boundary layer. Although typical boundary layer thicknesses are around 1 millimeter [8], a spore's small size (roughly 10 micrometers) causes rapid deceleration after launch, meaning that it must be launched at very high velocity even to travel a very small distance, and the likelihood of effective dispersal is directly correlated to the thickness of boundary layer that the spore is able to cross [9].

The critical role of the apical ring in spore dispersal caused speculation about whether the diverse morphologies of the spore ejection apparatus are tuned to allow effective dispersal. Buller proposed a relationship between the dimensions of the apical ring and the size of the spore, ostensibly to prevent spores from tumbling during flight [10]. Ingold thought spores would be shaped to maximize the force used by apical rings to push on them [7]. But, surprisingly, the individual geometric dimensions of apical rings and spores critical to these hypotheses are either very weakly or not correlated.

Here we resolve this discrepancy by demonstrating a strikingly tight coupling between the size of the spore and a nonlinear function of multiple dimensions of the apical ring. The relationship is suggested by physical constraints on spore ejection: the requirement to efficiently convert the potential energy stored in the ascus to kinetic energy of the spore. The apical ring is an elastic seal, and distorts significantly when the spore, which is lubricated by a thin fluid layer, passes through it. The basic physical principles governing this kind of process were discovered fifty years ago, in the study of elastomeric seals and O-rings used to control fluid flow in engines, pipes and other engineering applications [11]. By adapting these theories to the fluid mechanics of spore ejection, we demonstrate that although there are at least 5 independent dimensions to the morphological diversity of spores and apical rings, the need to minimize energy losses during ejection restricts spore and ascus morphologies to a one-dimensional subspace, where the dimensions of a spore and its apical ring are tightly coupled.

We test this theory using published electron micrographs of apical rings and spores (e.g. [12–19]) and a recently published ascomycete phylogeny [20], which identifies two potentially independent groups of species with spores singly ejected through apical rings. Quantitative descriptions of spores and apical rings at a high resolution are available for 45 species, with dimensions of the spore and apical ring characters varying over one order of magnitude. Nonetheless, the observed variation is confined to the predicted one-dimensional subspace with surprising accuracy: energy losses are held within two percent of the theoretical optimum.

By assembling data on species where there is no selective pressure to maximize ejection velocity, because spores are dispersed using different mechanisms, for example, insect vectors, we test whether genetics are a constraint on morphology. In fact, these species have very different apical ring and spore shapes, suggesting natural selection is the force maintaining collapse into the one-dimensional subspace for species with functional apical rings.

Results

Fluid Mechanics of Spore and Apical Ring Coupling

Fig. 1 shows a representative context in which spore ejection occurs. The sporocarps of a fungus are scattered on a host (e.g. the stalk of a plant, Fig. 1A). These structures are produced by the fungus with the sole purpose of dispersing the spores. Within each sporocarp, there can be hundreds of asci, each generally containing eight spores (Fig. 1B). When the spores in an ascus are mature, osmolytes are produced, leading to water influx into the highly elastic ascus, resulting in a significant increase of volume and pressure [4]. When the osmotic pressure p_0 inside an ascus is sufficiently high, the spores are singly ejected into the surrounding air.

The speed U at which a spore is launched depends critically on energy losses during ejection. If the osmotic pressure were entirely converted to kinetic energy, the spore would be ejected at an ideal velocity:

$$U_{ideal} = \sqrt{\frac{2p_0}{\rho_s}} \tag{1}$$

where ρ_s is the density of the spore and p_0 is the overpressure in the ascus.

However, the ideal launch velocity is necessarily degraded by both friction and fluid loss as the spore moves through the apical ring (Fig. 1C,D). The apical ring consists of an elastic material with thickness b and height ℓ. The size of the opening of the apical ring before the spore starts to pass through it, d, is much smaller than the width W of the spore. During the ejection of the spore, the apical ring is strongly deformed, and there is a thin layer of fluid with viscosity μ and density ρ, separating the apical ring from the spore.

Energy losses arise from two different processes occurring in this lubricating fluid layer of thickness h_0: first, there is friction between the spore and the

apical ring, due to the viscous force in the fluid gap $F \sim W\ell\mu U/h_0$, opposing the motion of the spore moving with velocity U. The total energy dissipated is then $E_{friction} = FL$, the product of this viscous force with the distance that the spore moves when the force is acting, which is the length L of the spore. The second energy loss arises because the pressure in the ascus, and thus the main accelerating force, decreases while the spore and lubricating fluid leave the ascus. If ascus pressure and volume are proportional, the energy lost due to fluid leaving the ascus is proportional to the kinetic energy, $E_{fluid} = \rho W h_0 L U^2$, up to a constant parameterizing the ratio of ascus volume before ejection to spore volume. If h_0 is large, the energy loss is dominated by the fluid flow through the gap, while if h_0 is small, the energy loss is dominated by friction. The minimal total energy loss $E_l = E_{fluid} + E_{friction}$ occurs if $E_{fluid} \approx E_{friction}$ and thus if the physical gap thickness is close to the optimal value $h_0 = h_*$, with

$$h_* = \alpha\sqrt{\frac{\mu\ell}{\rho U}} = \alpha\frac{(\mu\ell)^{1/2}}{(2\rho p_0)^{1/4}}, \tag{2}$$

where in the second equality, we have assumed that the energy dissipation is sufficiently small that $U \approx U_{ideal}$, with $\rho_s \approx \rho$. The proportionality factor $\alpha = 0.45$ can be found by explicitly integrating the equations of motion for the spore, as demonstrated in the electronic supplementary material (*ESM)*. Fig. 2A shows a plot of the energy dissipated as a function of h_0 following from this more complete analysis.

The fluid layer thickness h_0

What physical mechanism determines h_0? During spore ejection, the apical ring undergoes a strong deformation to allow the spore to pass, and this deformation causes a restoring elastic pressure to push against the spore. On the other hand, within the fluid gap there is viscous pressure caused by the fluid motion itself. The fluid layer thickness h_0 is determined so that these two pressures exactly balance. The layer thickness h_0 thus depends in a nontrivial fashion on all of the parameters of the problem outlined thus far: the dimensions and elastic modulus E of the apical ring, the viscous forces acting in the thin fluid layer, and the size of the spore.

Determining the dependence of the layer thickness h_0 on these parameters is a classic problem in elastohydrodynamics, and it was examined in the 1960's to understand the properties of engineering seals, for example O-rings. The theoretical ideas worked out in this context are directly applicable to the present problem, and here we recapitulate the basic arguments [11,21,22] in the context of our system. Fig. 1E shows the geometry of the contact, focusing on the edge of the apical ring where the spore enters from the ascus. The coordinate x parameterizes distance from the entry point, located at $x = 0$. Within the ascus, far from the spore entry point, the pressure is $p \approx p_0$, and the shape of the apical ring is undeformed.

First, it is convenient to consider what would happen if there were no fluid gap ($h_0 = 0$), and no flow through the contact. In this case, the elastic distortions and pressures caused by the spore moving through the apical ring follow from Hertzian contact theory. The Hertz contact solution is completely specified by the local radius of curvature $R_* \sim \ell$ of the contact region [1], and the resulting elastic deformation, implying that when $x < 0$, $h(x) = \xi(x/\xi)^{3/2}$, whereas when $x > 0$, the pressure distribution for $x/\xi \lesssim 1$ obeys $p(x) = E\sqrt{x/\xi}$, where $\xi = \ell\sqrt{E/p_r}$ is an elastic healing length. Here, p_r is the elastic pressure exerted by the spore on the apical ring, well inside the contact ($x/\xi \gg 1$). Since the ring deformation is dominated by the spore passing through it, we can neglect the deformation of the ascus wall for the elastohydrodynamic calculation. Under this assumption we can approximate the apical ring as a circular cylinder with internal radius $r_i = d/2$ and outer radius $r_o = d/2 + b$, subject only to an internal pressure p_r. Due to symmetry, the displacement of the ring depends only on the radial distance r from the center line. Classical elasticity theory [23] dictates that the deformation is given by

$$u = \frac{3}{2E}\frac{p_r r_i^2}{r_0^2 - r_i^2}\frac{r_o^2}{r}. \tag{3}$$

With the spore passing through the apical ring, the deformation of the inner surface of the ring is $u(r_i) = W/2$, implying the elastic pressure

$$p_r = \frac{E}{3}W\frac{r_o^2 - r_i^2}{r_i r_o^2} = E_* W\frac{b(d+b)}{d(d+2b)^2} \tag{4}$$

where $E_* = 2/(1-\nu^2)E = 8/3E$. Here we have assumed that the apical ring is incompressible (Poisson ratio $\nu = 1/2$), as are most biological materials.

With a fluid gap separating the apical ring from the spore, this purely elastic solution is modified. Dowson and Higginson [11] solved the coupled elastohydrodynamic problem by realizing that the fluid gap thickness h_0 itself only slightly increases the elastic distortion of the apical ring. The pressure distribution in the center of the apical ring is thus still given by the Hertzian solution, scaling as $p \sim E\sqrt{x/\xi}$ for $x \lesssim \xi$. Similarly, away from the contact (negative x in Fig. 1E), the shape of the apical ring is mainly affected by the large elastic stresses within the contact, and so it is also given by the Hertzian solution, $h \sim \xi|x/\xi|^{3/2}$. However, there will be deviations near the entry point ($x \approx 0$), where the fluid pressures created by the flow through the gap will significantly modify $h(x)$.

Solving for $h(x)$ in this regime requires coupling the viscous flow in the gap to the elastic deformation of the apical ring. Viscous forces imply that the pressure gradient in the gap is given by the Reynolds lubrication equation,

$$\frac{dp}{dx} = 6\mu U\frac{h - h_0}{h^3}, \tag{5}$$

[1] The local radius of curvature is approximately ℓ as a result of the spore being much larger than the apical ring. We obtain the proportionality constant by data analysis as illustrated in the *ESM*.

A coupled solution to the elastohydrodynamic problem requires that the pressure distribution $p(x)$ and the gap shape $h(x)$ satisfy *both* the Reynolds equation (5), and the elastic equations.

The value of h_0 is selected by the solution to this coupled elastohydrodynamic problem [11]. The dependence of h_0 on parameters follows from a scaling argument at $x \approx 0$ [21]. If λ is the length scale over which the pressure varies in the fluid gap, P is the pressure scale, and H is the scale of the gap thickness, Eq. (5) implies $P/\lambda \sim \mu U/H^2$. The lubrication solution must match the Hertz solutions, implying $P \sim E\sqrt{\lambda/\xi}$ and $H \sim \xi(\lambda/\xi)^{3/2}$. Combining these relations, we find that

$$h_0 = \beta H = \beta \frac{\xi}{K^{3/5}} = \beta \left(\frac{\mu^3 p_0^{3/2} \ell^2 d(d+2b)^2}{\rho^{3/2} E_*^3 W b(d+b)} \right)^{1/5}, \tag{6}$$

where $K = E_* \xi/(U\eta)$ is the ratio of the elastic modulus to the viscous pressure created in the gap. The proportionality constant $\beta = 1.42$ requires the complete elastohydrodynamic solution, outlined in the *ESM*. Fig. 2B shows the exact gap height and pressure following from this complete elastohydrodynamic analysis. Note that in order to effectively minimize the fluid loss through the gap, the pressure in the gap (for $x > 0$) will be significantly higher than in the ascus ($x << 0$). This is consistent with our previous assumption that the pressure in the ascus is the main accelerating force of the spore. The gap pressure acts nearly exactly perpendicular to the spore motion during the ejection of the spore and can thus be neglected when calculating its acceleration (see *ESM*).

Optimality Criterion

We can now combine the results of the last two sections to define an optimal spore shooting apparatus. To minimize energy losses during spore ejection, the thickness of the fluid gap (h_0, Eq. (6)) determined by the elastohydrodynamic solution must be close to the optimal thickness of the fluid gap (h_*, Eq. (2)). The equation $h_0 = h_*$ implies the law

$$W = \gamma \frac{\mu^{1/2}}{(p_0\rho)^{1/4}} \left(\frac{p_0}{E_*} \right)^3 \frac{d(d+2b)^2}{b(d+b)\sqrt{\ell}}, \tag{7}$$

where $\gamma = \gamma(\alpha, \beta) = 371$ (see *ESM* for derivation).

Testing the prediction with morphological data

Eq. (7) implies a strong constraint coupling spore and apical ring morphologies: the spore diameter W should be linearly proportional to a single parameter S_r, capturing the different dimensions of the apical ring,

$$S_r = \frac{d(d+2b)^2}{b(d+b)\sqrt{\ell}}, \tag{8}$$

if the material parameters of all species, most notably p_0/E_*, are reasonably conserved. While theoretical considerations make it likely that both these values individually should be roughly constant across different species (see *ESM*), no experiments determining the elasticity of apical rings have been performed. The few available measurements of p_0 for different species indicate that this value might be roughly conserved [24].

To test our prediction, we compiled a library of over 1000 papers from the mycological literature, and searched them for high resolution electron-micrograph images showing medial cuts of mature apical rings (see *ESM* for search rules and example images). We found data for 45 species in 2 classes (18 families), with a good coverage of the whole phylogeny of species whose spores are singly ejected through an apical ring (see Fig. 3, classes and families where data were found are shown in color). The phylogeny highlights the ubiquity of this trait in the ascomycetes (Fig. 3A), not only in two large classes (Fig. 3B,C) but also in more distant families (e.g. Peltigeracea and Geoglossacea), potentially indicating multiple independent origins of this trait. It also shows several loss events (represented by dashed lines), where species ejecting spores through an apical ring evolved into niches where this trait conveyed no selective advantage and was eventually lost, both on the class level (e.g. Laboulbeniales, Fig. 3A) and family level (Fig. 3B,C).

From the images found with this search we extracted the three independent dimensions of the apical ring (b, ℓ and d) relevant to our physical model, as well as the spore size W. When available, morphological data were taken from the same publication, to limit the influence of intraspecies variability. If no spore size was reported or could be measured, it was taken as the average value reported in standard texts [25, 26] (see *ESM* for details).

Fig. 4 shows the results of this analysis. Each data point represents one species from the classes highlighted in Fig. 3. The individual dimensions of the apical rings are not strongly linked to the dimensions of the spores for the same species. The spore width W does not correlate with ℓ or b (R-squared 0.11 and 0.10). The degree of correlation between W and d is higher (R-squared 0.64), indicating that species with larger spores have apical rings with slightly larger diameters. In contrast, Fig. 4B shows the correlation of the spore radius with S_r. The data collapse on a single straight line (R-squared 0.84) is in excellent agreement with the theoretical expectation (Eq. (7)), with only one free parameter $D = \gamma\mu^{1/2}(p_0/E_*)^3/(p_0\rho)^{1/4} = 0.79 \pm 0.06\,\mu\mathrm{m}^{1/2}$. If we assume $\rho = 1000\,\mathrm{kg/m^{-3}}$, $\mu = 10^{-3}\,\mathrm{Pa}\cdot\mathrm{s}$ and $p_0 = 2\,\mathrm{atm}$ [27], the predicted elastic modulus of the apical ring is $E_* \approx 1\,\mathrm{MPa}$, consistent with the elastic moduli of soft biological materials [28]. To quantify energy losses within this system, Fig. 4B also shows contours (gray shading) for spores attaining 99%, 98%, and 95% of the maximum launch velocity, which can be obtained from a numerical integration of the equations of motion (see *ESM*). Nearly all of the data fall within 2% of the theoretical optimum.

Discussion

The collapse of morphological data suggests spore launching apparatuses have evolved to maximize dispersal potential. A spore must escape its parent and if it can penetrate through the fluid mechanical boundary layer surrounding the sporocarp, it may be carried by the wind and achieve long distance dispersal. After launch from the ascus, the velocity $U(t)$ of a spore decelerates according to

$$m\frac{dU}{dt} = -\zeta U, \tag{9}$$

where m is the spore mass and ζ the drag coefficient. This implies that the distance Z a spore ejected with initial velocity U_{ej} will travel is given by

$$Z = U_{ej}\frac{m}{\zeta}. \tag{10}$$

The larger the range Z, the greater the variety of environments a spore can tolerate and still escape the boundary layer. We have previously shown the shape of spores (the ratio m/ζ) is tuned to within 1% of the theoretical optimum [29]; the present study demonstrates that the launch velocity U_{ej} is optimized to the same degree of precision by matching apical ring shape to spore size.

Our theory shows that gradients away from the optimum are steep – if a species moves off of the line in Fig. 4B, the energy dissipation penalty will be high, and the launch velocity U_{ej} will plummet.

The most striking feature of the data collapse shown in Fig. 4B is the large diversity of apical ring shapes captured by the model. Apical rings may be flat, thin, elongated, or shallow, with only weak correlations between the different geometrical dimensions, as seen in Fig. 3D (R-squared between 0.32 and 0.39), but in the right combination all morphologies are confined to the one dimensional subspace of the theoretical prediction (Eq. (7)). It is worth noting that our analysis explains more of the variation in the dimensions W, d, ℓ, b than traditional morphometric analysis using the first principal component (84 vs 64%). Principal component analysis finds the linear combination of parameters that best explains a wide variance. In contrast, Eq. (7) depends nonlinearly on all of the parameters, in a fashion predicted by our mechanical analysis of dissipation processes occurring during spore ejection (see *ESM*).

Morphologies may also be shaped by genetic constraints. To test whether genetics constrains fungi within the one-dimensional subspace, we explored the evolutionary trajectories of ascomycete species not subject to the selective force for range maximization. Several groups have evolved into niches where spore shooting is not critical to survival, because species use insects or other animals to disperse spores. Although nearly all of these species have completely lost the apical ring, the evolutionary residue of spore ejection is seen in a few genera, for example, *Geospora*. Species of *Geospora* do forcibly eject spores, but spores are ejected into a closed, subterranean sporocarp, where range maximization is irrelevant.

Using the same methodology described for the forcibly ejecting species (see *ESM* for details) we collected morphological data for 13 species with non-functional rings: 7 are deliquescent i.e. ascospores are not forcibly ejected because the ascus wall dissolves; 5 are cleistothecial i.e. spores are released within an enclosed sporocarp; and one releases spores through a fissure in the ascus wall, and not through the apical ring. The spore and ring morphologies of 9 of 13 species are far from the subspace occupied by spore-shooting species (see Fig. 5). So while over 90% of all species with functional apical rings have morphologies within 2% of the optimum, this is only the case for about 30% of species with non-functional apical rings.

These data confirm that the data collapse in Fig. 4B is not the result of genetic constraints: alternate morphologies are possible. In fact, the time of divergence from an ancestor with a functional apical ring is positively correlated with the loss of optimality of the apical ring (see inset of Fig. 5), suggesting a role for genetic drift in shaping these morphologies. In a phylum with almost no fossil record, and where molecular clock models remain problematic, morphological trait evolution may provide valuable additional data for dating species divergences.

Our model highlights the key role of physics in generating and shaping morphological diversity, which – even despite the emergence of molecular tools – remains a key to understanding the evolution of biodiversity.

Materials and Methods

Integration of equations of motion

If ascus pressure p_a and ascus volume covary linearly[2], then Eq. (6), the pressure evolution equation, and Newton's equation for the spore form a closed system of equations that can be written in non-dimensional form as

$$U\frac{dU}{dX} = 3X(1-X)p_a - \frac{12}{\beta}\frac{G}{F}U^{2/5}[X(1-X)]^{6/5} \tag{11}$$

$$\frac{dp_a}{dX} = -\frac{48}{C}[X(1-X) - \beta FGU^{3/5}(X(1-X)]^{4/10} \tag{12}$$

where X,U and p_a are normalized by L,U_{id} and p_0 respectively. The value of $U_{ej} = U(X = 1)$ after integration only depends on the three non-dimensional parameters $G = h_*/W$,$F = H/h_*$ and C, which is the ration of ascus to spore volume before ejection (see *ESM* for details). In the physiologically relevant region of parameter space, the solution has a sharp optimum in F, corresponding to the optimum in h shown in Fig. 2A.

[2]Experimental evidence shows that they do covary during spore ejection [32] and linear covariance is most plausible given the material properties of the ascus in the relevant parameter regime(see *ESM*). For a different functional relationship our model still predicts $W \propto S_r$, however the interpretation of the constant of proportionality, and thus our prediction for the elastic modulus of the ring would change.

Elastohydrodynamics

Near the entry point, elasticity theory [11] dictates that the gap thickness is related to the pressure distribution by

$$h(x) - h_{\mathrm{Hertz}}(x) = \frac{3}{4\pi E}\int_{\infty}^{\infty} ds(p_f(s) - p_{\mathrm{Hertz}}(s)) \log \frac{|x-s|}{\xi}, \qquad (13)$$

where $h_{\mathrm{Hertz}}(x), p_{\mathrm{Hertz}}(x)$ are the Hertz solutions, and p_f is the solution to the Reynolds equation (5). We require $p_f(x) \sim p_{\mathrm{Hertz}}$ far from the entry point, i.e as x becomes large. For this to happen, the gap thickness must asymptote to a constant value $h \to h_0$. We solve Eq. (13) iteratively at every point x along the contact profile (for details see *ESM*) to compute the pressure and hight profile shown in Fig. 2B.

Acknowledgments

We thank the Harvard Botany Libraries for their help and M. Mani, T. Schneider and D. Pfister for useful discussions and comments. We also thank three anonymous referees for their positive and extremely helpful feedback that significantly improved the quality and clarity of this paper. This research was supported by the National Science Foundation through the Harvard Materials Research Science and Engineering Center (DMR-0820484) and the Division of Mathematical Sciences (DMS-0907985), by the National Institute of General Medical Sciences (GM-068763), by a Marie Curie IO Fellowship within the 7th European Community Framework Programme to AS, and by a fellowship from the Alfred P. Sloan Foundation to MR. MPB is an investigator of the Simons Foundation.

References

[1] Fisher MC, Henk DA, Briggs CJ, Brownstein JS, Madoff LC, McCraw SL, Gurr SJ. 2012 Emerging fungal threats to animal, plant and ecosystem health. *Nature* **484**, 186-194

[2] Pennisi E. 2010 Armed and Dangerous. *Science* **327**, 804-805.

[3] Trail F, Xu H, Loranger R, Gadoury D. 2002 Physiological and environmental aspects of ascospore discharge in Gibberella zeae (anamorph Fusarium graminearum). *Mycologia* **94**, 181-189.

[4] Trail F, Gaffoor I, Vogel S. 2005 Ejection mechanics and trajectory of the ascospores of Gibberella zeae (anamorph Fusarium graminearum). *Fungal. Genet. Biol.* **42**, 528-533.

[5] Linnaeus C. 1753 *Species plantarum.* Stockholm: Impensis Laurentii Salvii.

[6] DeBary A. 1887 *Comparative Morphology and Biology of the Fungi, Mycetozoa and Bacteria.* Oxford, U.K.: Clarendon Press.

[7] Ingold C. 1971 *Fungal Spores: Their Liberation and Dispersal*. Oxford, U.K.: Clarendon Press.

[8] Batchelor G. 1967 *Introduction to Fluid Dynamics*. Cambridge, U.K.: Cambridge University Press,.

[9] Roper M, Seminara A, Bandi MM, Cobb A, Dillard H, Pringle A. 2010 Dispersal of fungal spores on a cooperatively generated wind. *Proc. Natl. Acad. Sci. U.S.A.* 107, 17474-17479

[10] Buller A. (1934) *Researches on Fungi, Vol 6*. New York: Longmans & Green.

[11] Dowson D, Higginson GR. 1959 A numerical solution to the elasto-hydrodynamic problem. *Journal of Mechanical Engineering Science* **1**, 5-15.

[12] Greenhalgh GN, Evans LV. 1967 The structure of the ascus apex in Hypoxylon fragiforme with reference to ascospore release in this and related species. *Transactions of the British Mycological Society* **50**, 183-188.

[13] Griffiths HB. 1973 Fine structure of seven unitunicate pyrenomycete Asci. *Transactions of the British Mycological Society* **60**, 261-271.

[14] Beckett A, Crawford RM. 1973 The Development and Fine Structure of the Ascus Apex and its Role During Spore Discharge in Xylaria longipes. *New Phytol.* **72**, 357-369.

[15] Corlett M, Elliott ME. 1974 The ascus apex of Ciboria acerina. *Can. J. Bot.* **52**, 1459-1463.

[16] Honegger R. 1978 The Ascus Apex in Lichenized Fungi I. The Lecanora-, Peltigera- And Teloschistes-Types. *The Lichenologist* **10**, 47-67.

[17] Verkley GJM. 1992 Ultrastructure of the apical apparatus of asci in Ombrophila violacea, Neobulgaria pura and Bulgaria inquinans (Leotiales). *Persoonia* **15**, 3-22.

[18] Verkley GJM. 1994 Ultrastructure of the apical apparatus in Leotia lubrica and some Geoglossaceae (Leotiales, Ascomycotina). *Persoonia* **15**, 405-430.

[19] Verkley GJM. 2003 Ultrastructure of the ascus apical apparatus and ascospore wall in Ombrophila hemiamyloidea (Helotiales, Ascomycota). *Nova Hedwigia* **77**, 3:271-285.

[20] Schoch CL *et al* 2009 The Ascomycota Tree of Life: A Phylum-wide Phylogeny Clarifies the Origin and Evolution of Fundamental Reproductive and Ecological Traits. *Syst Biol* **58**, 224-239.

[21] Hooke CJ, Donoghue JP. 1972 Elastohydrodyamic lubrication of soft, highly deformed contacts *Journal of Mechanical Engineering Science* **14**, 34-48.

[22] Dowson D. 1995 Elastohydrodynamic and micro-elastohydrodynamic lubrication *Wear* **190**, 125138.

[23] Little RW. 1973 *Elasticity*. Englewood Cliffs, NJ: Prentice Hall.

[24] Trail F. 2007 Fungal cannons: explosive spore discharge in the Ascomycota. *FEMS Microbiol. Lett.* 276, 8-12.

[25] Dennis RWG. 1978 *British ascomycetes*. Vaduz: Cramer.

[26] Breitenbach J, Kränzlin F. 1984 *Fungi of Switzerland: Ascomycetes*. Lucerne: Verlag Mykologia.

[27] Fischer M, Cox J, Davis DJ, Wagner A, Taylor R, Huerta AJ , Money NP. 2004 New information on the mechanism of forcible ascospore discharge from Ascobolus immersus. *Fungal. Genet. Biol.* **41**, 698-707.

[28] Knowles T, Buehler MJ. 2011 Nanomechanics of functional and pathological amyloid materials. *Nature Nanotechnology* **6**, 469-479.

[29] Roper M, Pepper RE, Brenner MP, Pringle A. 2008 Explosively launched spores of ascomycete fungi have drag minimizing shapes. *Proc. Nat. Acad. Sci. USA* **105**, 20583-20588.

[30] Thongkantha S *et al.* 2009 Molecular phylogeny of Magnaporthaceae (Sordariomycetes) with a new species, Ophioceras chiangdaoense from Dracaena loureiroi in Thailand. *Fungal Divers.* **34**, 157-173.

[31] Campbell J, Anderson JL, Shearer CA. 2003 Systematics of Halosarpheia Based on Morphological and Molecular Data. *Mycologia* **95**, 530-552.

[32] Ingold CT. 1961 Ballistics in Certain Ascomycetes. *New Phytol.* **60**, 143-149.

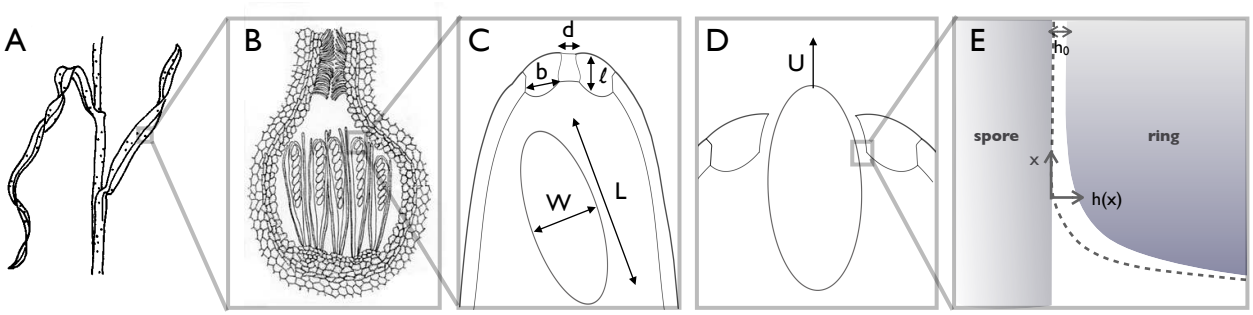

Figure 1: The spore shooting apparatus. (A) Sporocarps on the stalk of a plant. (B) Flask-shaped sporocarp, containing 5 asci. (C) Upper part of an ascus with a mature spore close to the apical ring, which is still sealed. The length L and width W of the spore and the dimensions of the apical ring (ℓ, b, d) are indicated. (D) Spore moving at velocity U and deforming the apical ring at launch. A lubricating layer of fluid separates the spore from the ring. (E) The region where the spore first deforms the ring. x measures the distance from the point where the spore starts to compress the ring; the gap thickness h varies with x and asymptotes to a constant value h_0 at $x > \lambda$ as described in the text. Dashed line: dry contact deformation.

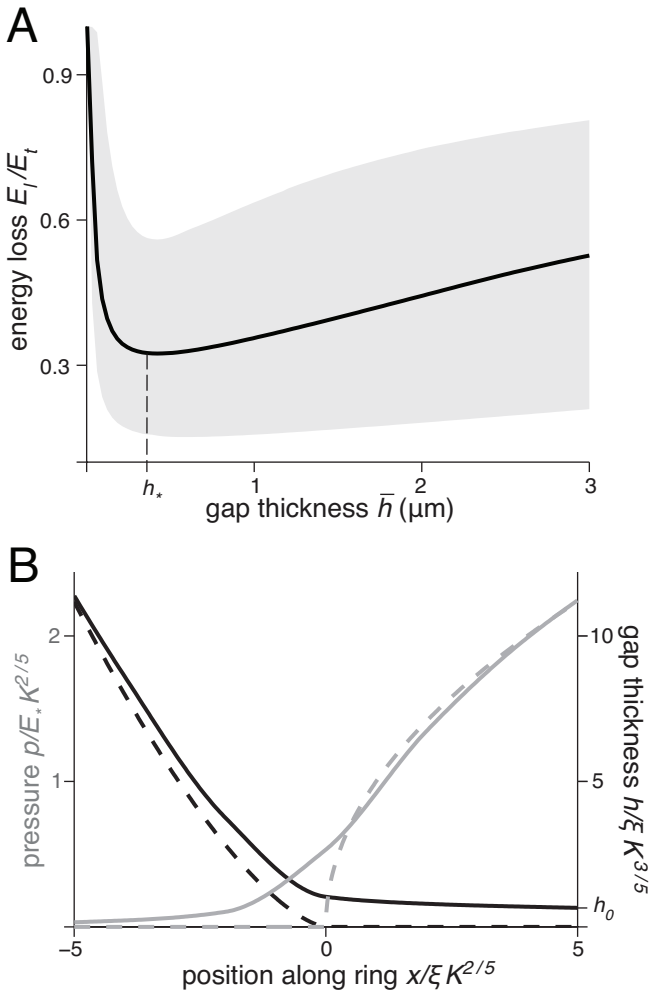

Figure 2: Simulations of the elastohydrodynamics of apical ring deformation coupled with spore motion shows the optimal thickness h^* (Eq. (2)). (A) Total energy dissipated through friction and fluid loss $E_l = E_{fluid} + E_{friction}$, as a function of the average gap thickness $\bar{h}$. We normalize E_l with the final spore kinetic energy $E_t = 2LW^2\rho U_{ej}^2/3$. Energy dissipation is minimized at the optimal gap thickness h_*, which is preserved as we vary the parameters of the model (G, C described in the *ESM*). Solid lines/shades: results obtained for a realistic set of parameters ($G = 0.05$, $C = 2.3$, $D = 0.79\,\mu m^{1/2}$) and their expected variation, as described in the *ESM*. (B) Normalized gap thickness (black) and pressure (grey) as a function of the distance from the point $x = 0$ where the spore first starts to compress the ring. The appropriate non-dimensionalization and numerical procedure are described in the *ESM*. Dashed lines: solution of the dry contact problem; solid lines: solution of the full elastohydrodynamic problem.

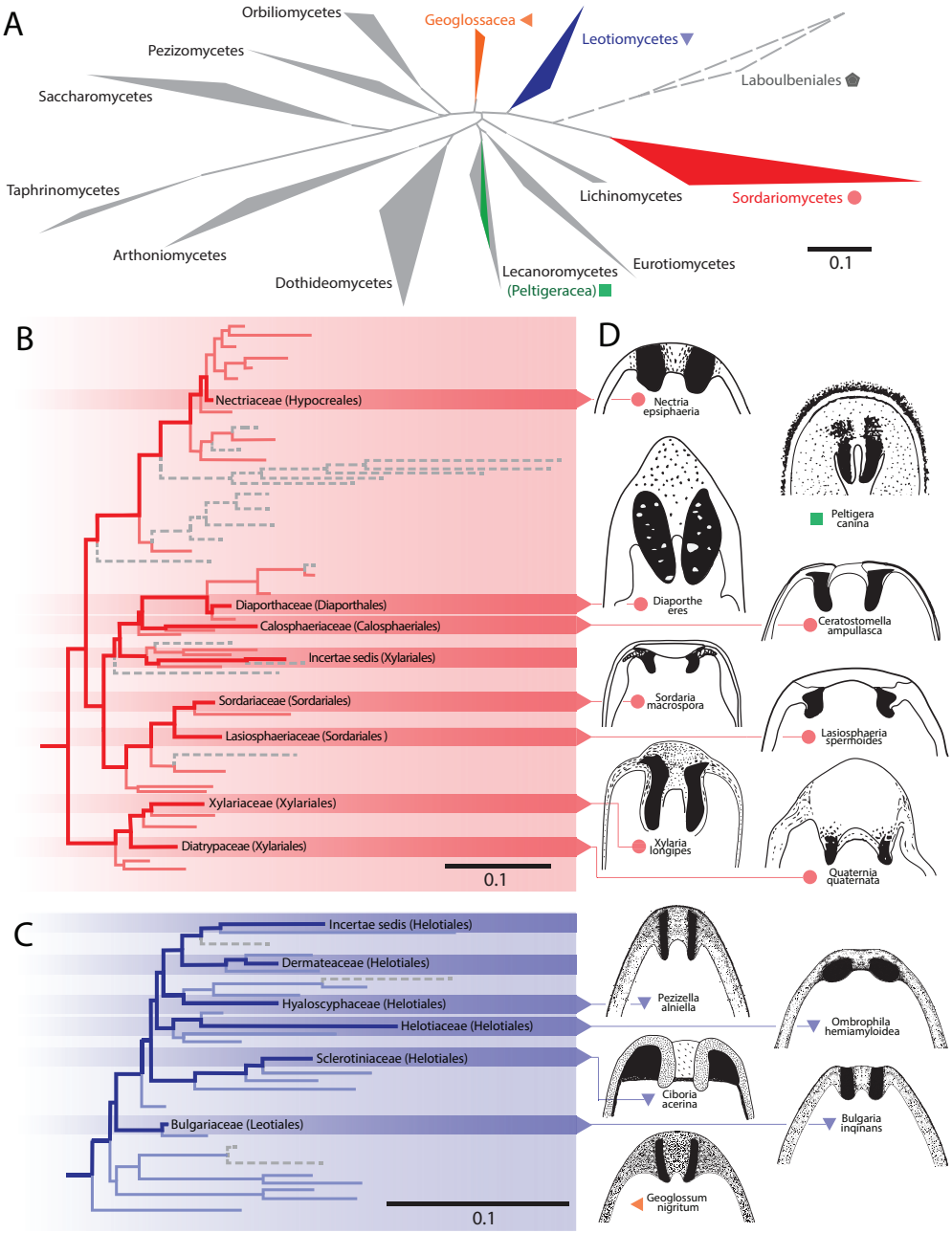

Figure 3: Phylogenetic tree highlighting the 45 species used in this study (adapted from [20]). Classes and families with functional apical rings are in color, those with non-functional rings are represented by gray dashed lines, and classes with other dispersal mechanism are shown in solid gray. (A) Cladogram of the entire ascomycete phylum, delineating classes. Clades with functional apical rings are the Leotiomycetes (blue), Sordariomycetes (red), Geoglossaceae (orange) and the Peltigeracea in the Lecanoromycetes (green). More detailed phylogeny of the Sordariomycetes (B) and of the Leotiomycetes (C) delineating families. The families of the species used in this study are highlighted. (D) Examples of apical ring geometries (not to scale) to illustrate morphological diversity (redrawn from [12–19]). Scale bars represents substitutions per site.

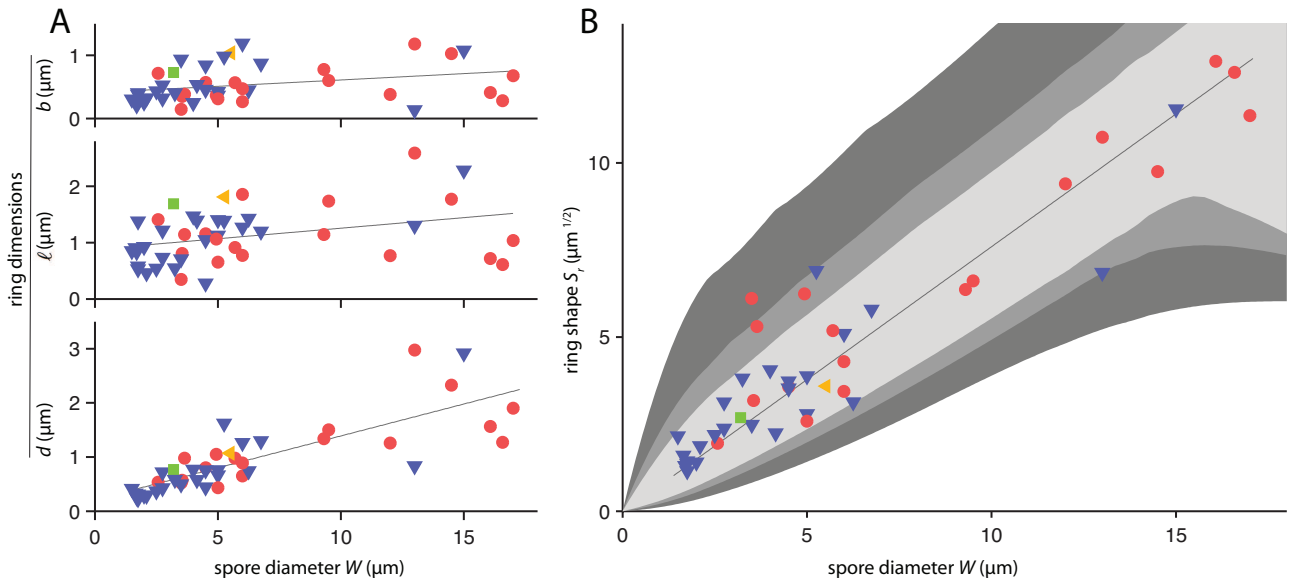

Figure 4: Comparison between the theoretical prediction and real morphological data for 45 species represented in Fig. 3 by matching colors and symbols. (A) Correlation between the width of the spore W and individual dimensions of the ring. The R-squared values of the correlations are 0.11, 0.10, 0.64 for ℓ, b, d respectively. (B) The non-trivial combination of lengthscales predicted theoretically correlates well with spore width (R-squared value 0.84). The line represents Eq. (7) with fitting parameter $D = 0.79\,\mu m^{1/2}$. Contour lines represent regions where spores attain 99% (light grey) 98% (grey) 95% (dark grey) of the maximum ejecion velocity.

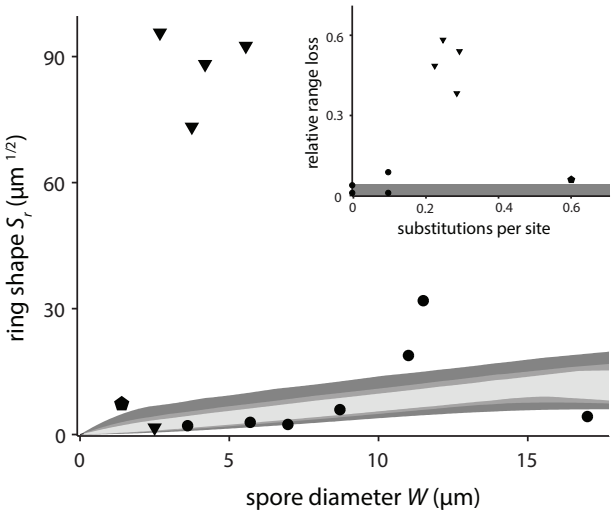

Figure 5: Morphological analysis for 13 species with non-functional apical rings. Symbols represent classes (see Fig. 3), species shown here are represented by dashed gray lines in Fig. 3. Contours as in Fig. 4B. Relaxation of the evolutionary constraint on the apical ring results in loss of optimality. No signature of the linear relation between W and S_r, as predicted by Eq. (7) for functional apical rings, can be seen here (R-squared 0.076; p-value 0.32). The (inset) shows a positive correlation between the phylogentic distance from the last ancestor with a functional apical ring (in substitutions per site) and the loss in range compared to an optimal ring geometry for the same spore size $(Z_{opt} - Z)/Z_{opt}$. The distance from the last common ancestor is measured on species level phylogenies [30, 31] using ancestral character reconstruction. The gray band corresponds to a 5% deviation from the optimum, which would contain all species with function apical rings. Note that 3 species are not shown in the inset, since their phylogenetic status in unclear.